Available online at www.CivileJournal.org

Civil Engineering Journal

Vol. 6, No. 9, September, 2020

Performance of Concrete Beams Reinforced with Various Ratios of Hybrid GFRP/Steel Bars

Phan Duy Nguyen [a*], Vu Hiep Dang [b], Ngoc Anh Vu [a]

[a] *Mientrung University of Civil Engineering, 24 Nguyen Du str., Ward 7, Tuyhoa City, 620000, Viet Nam.*

[b] *Hanoi Architectural University, Km10 Nguyen Trai str., Thanhxuan, Hanoi, 100000, Viet Nam.*

Received 25 May 2020; Accepted 03 August 2020

Abstract

This paper aims to study the flexural behavior of concrete beams reinforced with hybrid combinations of GFRP/steel bars. To this purpose an experimental program was carried out on four concrete beams reinforced with Glass Fiber Reinforced Polymer (GFRP) and twelve hybrid GFRP/steel Reinforced Concrete (RC) beams. Flexural behavior of the tested beams such as stages of response, failure modes, crack patterns, stiffness, toughness and ductility were analyzed. The experimental results showed that depending on GFRP/steel reinforcement configurations, the behavior of hybrid GFRP/steel RC beams undergoes three or four stages, namely: pre-cracking stage; after concrete cracking and before steel yielding; post-yield stage of the steel bar until peak load and failure stage. Totally six failure modes of hybrid RC beams are reported depending on reinforcement rations and configuration. The effect of reinforcement configuration and ratio of GFRP to steel (ρ_g) on the crack patterns, stiffness, ductility and toughness of hybrid RC beams are significant. Based on the non-linear deformation model, an analytical model has been developed and validated to determine the steel yielding moment and ultimate moment of hybrid GFRP/steel RC beams. It could be seen that the experimental values were in good agreement with the predicted values.

Keywords: Concrete Beam; Hybrid Reinforcement; Flexural Strength; Failure Mode; Fiber Reinforced Polymers.

1. Introduction

Damage, reduced service life and failure of concrete structures reinforced with steel bars are inevitably the most common consequences of steel reinforcement corrosion. Chloride ions, present in marine environment and seawater, are considered the main external agent to damage RC structures. The use of nonmetallic reinforcement, i.e. Fiber Reinforced Polymer (FRP), as an alternative reinforcement in concrete structures has emerged as a new solution owing to their non-corrosive and non-magnetic properties. However, due to the low modulus of elasticity of FRP, especially GFRP, there is a significant decrease in the bending stiffness of concrete members reinforced with FRP bars. Furthermore, the fact that the stress-strain relationship of GFRP bars is linear up to failure leads to a brittle failure mode of GFRP RC beams without warning. In order to overcome the drawbacks of individual use of the GFRP reinforcement, the hybrid combination of GFRP and steel reinforcement was introduced in concrete structures. These members could be divided into two groups: members created from existing concrete structures strengthened with GFRP bars; members formed by using simultaneously steel and GFRP bars in new-built concrete structures. For later case, GFRP rebars are placed closer to the concrete surface of the tensile zone with a small cover thickness whereas steel bars are placed with relatively larger concrete cover for a better protection against corrosion. Otherwise, the

* Corresponding author: nguyenphanduy@muce.edu.vn

http://dx.doi.org/10.28991/cej-2020-03091572

brittle behavior and low modulus of elasticity of GFRP reinforcement can be compensated by the presence of steel bars that can improve the ductility of structures.

Regarding the flexural behavior of concrete beams internally reinforced with hybrid reinforcement, Leung and Balendran [1] tested totally five hybrid over-reinforced concrete beams with two different concrete compressive strengths of 30 MPa and 50 MPa. The results indicated that the over-reinforced beams embedded with hybrid reinforcements introduced typical concrete crushing failure mode and no significant change in deflection at failure time. In the literature [2], Qu Wenjun et al. took out experimentally and theoretically investigation on the load-deflection behavior of concrete beams reinforced with hybrid GFRP/steel bars. Their theoretical model was based on the moment-curvature relationship of cross sections to predict the load-deflection relationship of the beams. They suggested that to estimate accurately the flexural performance of hybrid concrete beams, the tension stiffening effect should be included in the theoretical model at various load levels. Lau and Pam [3] investigated the ultimate strength and the ductility of hybrid GFRP/steel RC beams. The experimental results reported that the flexural ductility of pure GFRP RC members can be enhanced by two methods: by increasing the degree of over-reinforcement and by adding conventional steel rebars. To study the contribution of steel bars to behavior of hybrid GFRP/steel concrete beams, Mustafa and Hilal [4] used the nonlinear finite element program (ANSYS software). The results showed that the effect of steel bars on the behavior of hybrid concrete beams is considerably positive. The presence of steel bars improved beam ductility as well as the ultimate capacity after cracking. Similar to the researches mentioned above, the failure mode of almost hybrid concrete beams is first yielding in steel bars then crushing in concrete of compression zone. This is a typical failure mechanism found in previous many studies [1, 5, 6]. In fact, there may still be several modes of failure in hybrid GFRP/steel concrete beams that have not been reported and this study fills the gap by focusing on those failure modes.

To assess the ductility of reinforced concrete structures, it is common to use displacement ductility (μ_{Δ}) or curvature ductility (μ_{Φ}). However, because the mechanical properties of steel and GFRP are very different, evaluating the ductility of GFRP/steel hybrid reinforced concrete members by using displacement ductility or curvature ductility may lead to inconsistent outcomes. An energy-based ductility assessment approach can solve this problem. For instance, Bui et al. [7] evaluated the ductility of the FRP/steel RC beams considering the effects of the FRP on the steel reinforcement ratio and effects of the location of the FRP reinforcement on the mechanical performance of the beams. The results of this research showed that the ductility defined by absorption energy was different from that using the ductility factor defined as the conventional steel RC beams since the post-yield behavior of hybrid FRP/steel beams was almost decided by FRP reinforcement. The experimental results of Maranan et al. [8] also depicted that there was a contradiction of ductility between using the displacement ductility and energy-based ductility, the increase in displacement ductility could result in the decrease in energy absorption. Therefore, more research on ductility of concrete members reinforced with FRP/steel reinforcement is still necessary to cover this aspect. In addition, to the best of authors' knowledge the ductility classification of hybrid GFRP/steel concrete beams has not been mentioned.

At present, the majority of researches on flexural tests of hybrid GFRP/steel RC beams mainly focuses on evaluating bearing capacity load and deflection under service loading. Several studies on establishing the model for predicting moment capacity, deflection, curvature of hybrid FRP/steel RC beams and crack widths were presented [6, 9-11]. These researches revealed that the GFRP to steel ratio affects importantly the flexural performance and crack development of hybrid reinforced concrete beams. Recently, Sun et al. [12] carried out an experimental work on concrete beams reinforced with BFRP/steel in different arrangement of the longitudinal bars, i.e. bundled and distributed reinforcements. The results indicated that the secondary stiffness of beams still increase steadily. However, the effect of FRP to steel ratio on secondary stiffness of the tested specimens was not considered. Furthermore, the other key aspects related to bending behavior such as ductility based on energy, toughness have received little attention in the literature.

In this paper, to identify the failure modes of hybrid GFRP/steel RC concrete beams, twelve hybrid GFRP/steel RC beams and four GFRP RC beams with different reinforcement configurations were tested first. Then, the relationship between midspan deflection and load, stages of flexural behavior, failure modes, crack patterns at failure, stiffness, ductility index, toughness, load-carrying capacity and steel yielding load were analyzed. Finally, the predicted model of flexural behavior adopted from deformation models of materials was introduced and compared with the experimental results.

The rest of the article is structured as follows: Section 2 describes the experimental program of the hybrid GFRP/steel and GFRP RC beams; Section 3 presents test results and discussion in terms of global behavior, crack patterns, flexural stiffness, ductility index, toughness and moment carrying capacity in detail; Section 4 illustrates an analytical model to estimate the steel yielding moment and moment carrying capacity of hybrid beams; and the conclusions are given in the final section. The research flow chart is shown in Figure 1.

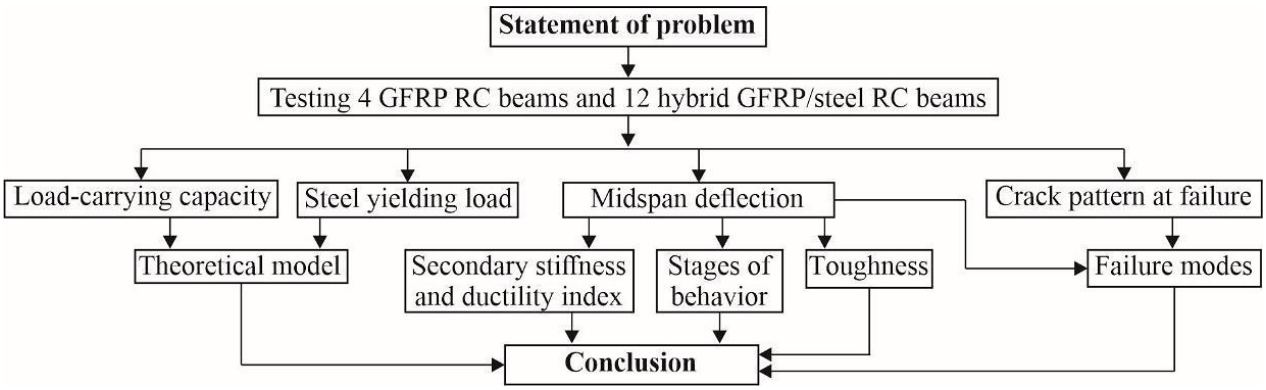

Figure 1. Flow chart of the research study

2. Experimental Study

2.1. Specimen Details

The testing beams were all designed as simply supported beams with a rectangular cross-section (150×250 mm). The total length (l) of the beam was 2700 mm. The testing span (l_0) was 2400 mm, of which the pure bending length was 400 mm (Figure 2).

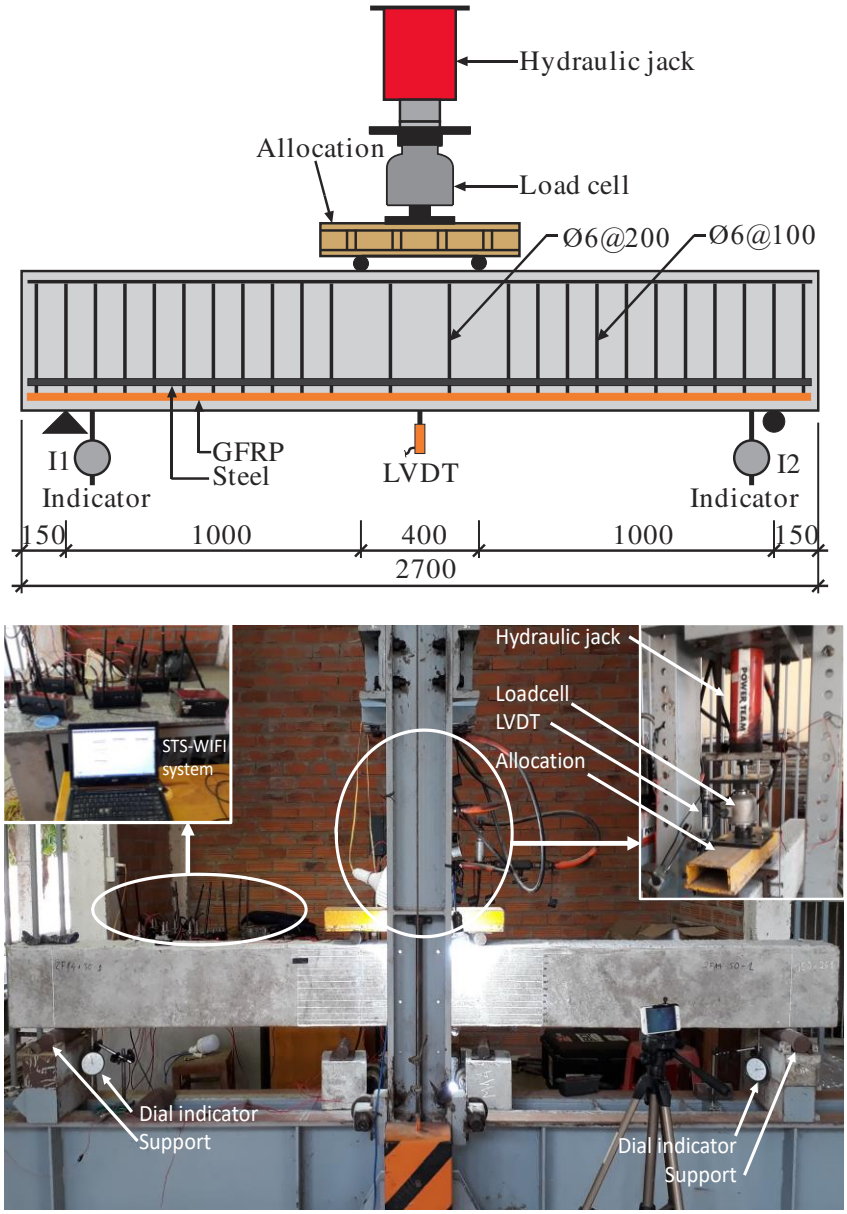

Figure 2. Beam design and loading scheme (Unit: mm)

The concrete beams reinforced with GFRP and hybrid GFRP/steel reinforcement were designed with reference to ACI 440.1R-15 [13]. In hybrid GFRP/Steel RC beams, the GFRP bars are located closer to the surface with the cover thickness (C_g) of 20 mm while the steel rebars are located deeper with the cover thickness (C_s) of 50 mm (Figure 3). Two steel bars of 6-mm diameter were used as reinforcement at the compression zone with concrete cover of 20 mm. The stirrups were made of steel plain round bars with a diameter of 6 mm, which had 100 mm spacing in shear span to avoid shear failure and a 200 mm spacing in midspan. The deformed steel bars with diameters of 10 mm, 12 mm, 14 mm and the GFRP bars with transverse spiral grooves with diameters of 10 mm, 12 mm and 14 mm are used as tensile reinforcement.

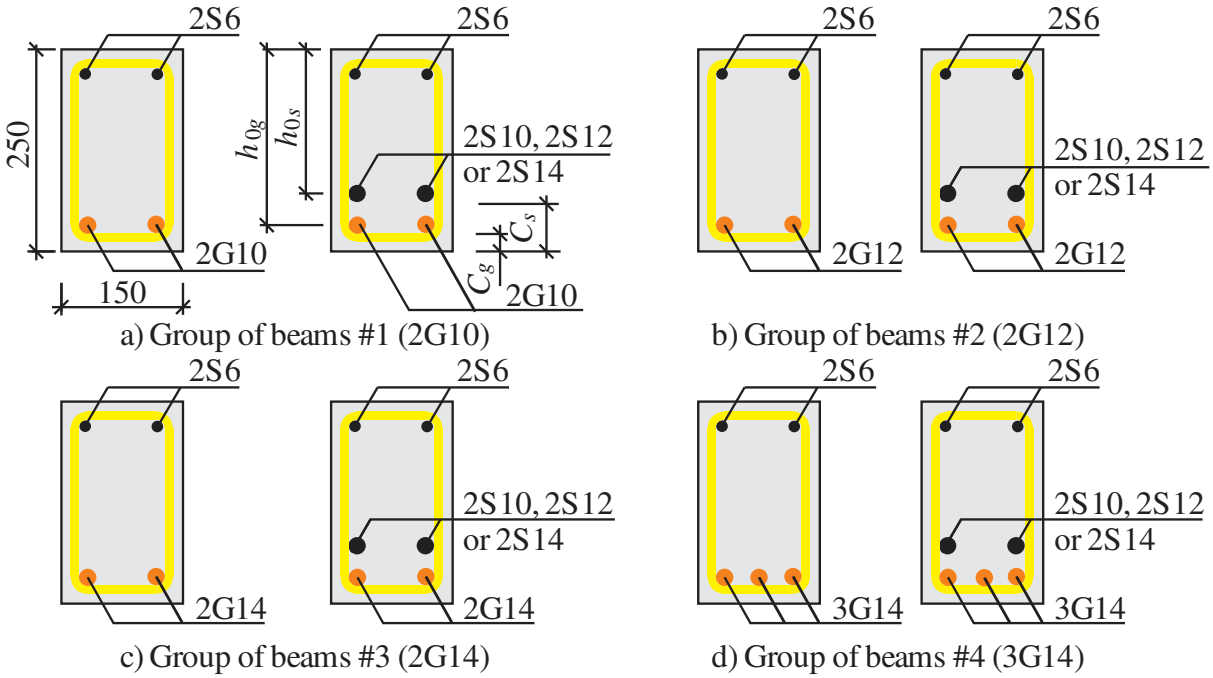

Figure 3. Cross sections of testing beams (Unit: mm)

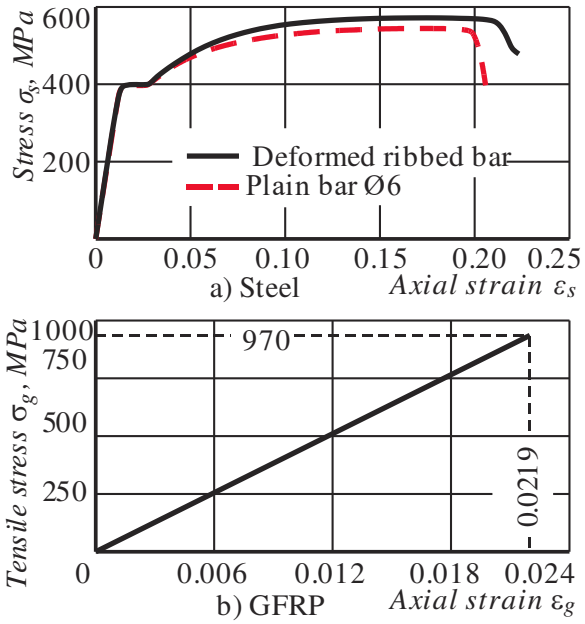

Figure 4. Stress-strain diagrams [14]

The beams were designed so that all possible failure modes may occur except the case of steel over reinforcement. The testing beams varied in the GFRP and steel reinforcement ratios and were divided into four groups. In each group, the GFRP reinforcement ratio μ_g was fixed (Group #1 – 2G10; Group #2 – 2G12; Group #3 – 2G14 and Group #4 – 3G14) and steel reinforcement ratios μ_s increased from about 0% to 1.13%. According to preliminary calculation results following ACI 440.1R-15 [13], the balanced reinforcement ratio for GFRP RC beam was 0.4%, hence the

GFRP reinforcement ratios used for testing beams varied from 0.36% to 1.16%. The actual dimensions, the concrete covers and reinforcement ratios of each beam will be measured and determined at the time of casting and experiment. Details of testing beams are given in Table 1. During the analysis of the experimental results, to evaluate the effect of the GFRP reinforcement on the characteristics of beams, the groups of hybrid RC beams with fixing steel reinforcement and varying GFRP reinforcement will be created: group of beams 2S10 (2G10-2S10; 2G12-2S10; 2G14-2S10 and 3G14-2S10); group of beams 2S12 (2G10-2S12; 2G12-2S12; 2G14-2S12 and 3G14-2S12); group of beams 2S14 (2G10-2S14; 2G12-2S14; 2G14-2S14 and 3G14-2S14) and group of beams S0 (2G10-S0; 2G12-S0; 2G14-S0 and 3G14-S0).

Table 1. Details of testing beams

Group of beams	Beam ID	b, mm	h, mm	C_g, mm	C_s, mm	h_{0g}, mm	h_{0s}, mm	A_g, cm^2	A_s, cm^2	R_m, MPa	μ_s,%	μ_g,%	μ_t,%
#1 (2G10)	2G10-S0	151	253	21	-	227	-	1.23	-	39.0	-	0.36	0.36
	2G10-2S10	152	254	25	49	224	200	1.23	1.57	41.6	0.52	0.36	0.88
	2G10-2S12	155	252	20	53	227	193	1.23	2.26	43.1	0.76	0.35	1.11
	2G10-2S14	150	253	28	54	220	192	1.23	3.08	39.2	1.07	0.37	1.44
#2 (2G12)	2G12-S0	151	249	16	-	227	-	1.87	-	44.2	-	0.55	0.55
	2G12-2S10	150	250	25	50	219	195	1.87	1.57	41.0	0.54	0.57	1.11
	2G12-2S12	155	250	20	45	224	199	1.87	2.26	37.4	0.73	0.54	1.27
	2G12-2S14	151	248	23	55	219	186	1.87	3.08	38.6	1.10	0.57	1.67
#3 (2G14)	2G14-S0	150	256	31	-	218	-	2.65	-	44.0	-	0.81	0.81
	2G14-2S10	151	251	24	47	220	199	2.65	1.57	41.0	0.52	0.8	1.32
	2G14-2S12	148	250	16	48	227	196	2.65	2.26	44.3	0.78	0.79	1.57
	2G14-2S14	153	255	26	55	221	192	2.65	3.08	43.2	1.06	0.79	1.85
#4 (3G14)	3G14-S0	148	255	19	-	229	-	3.97	-	45.5	-	1.17	1.17
	3G14-2S10	152	254	28	47	219	202	3.97	1.57	40.9	0.51	1.19	1.70
	3G14-2S12	153	254	23	48	224	200	3.97	2.26	41.0	0.74	1.16	1.90
	3G14-2S14	155	255	16	51	232	197	3.97	3.08	42.9	1.01	1.11	2.12

Note: 1) The capital letters G and S denote the steel bar and GFRP bar respectively; b and h – the average width and height of the cross section at midspan respectively; 2) The notation of 2G10-2S12 represents the beam's reinforcement with 2 GFRP bars in diameter of 10 mm and 2 steel bars in diameter of 12 mm; 3) C_g and C_s are the distances from bottommost concrete fiber to the nearest surface of GFRP and steel bars (concrete covers) respectively; h_{0g} and h_{0s} are the distances from outermost compressive concrete fiber to the centroid of GFRP and steel bars respectively; A_g and A_s are the areas of the cross section of GFRP and steel bars respectively; $\mu_s=A_s/(b\times h_{0s})$, $\mu_g=A_g/(b\times h_{0g})$ and $\mu_t=\mu_s+\mu_g$ are the steel, GFRP and total reinforcement ratio respectively.

The average cubic compressive strength R_m of concrete of each beam is evaluated by test on six cubic specimens (150×150×150 mm) after 28-days of curing (Table 1). GFRP bars used for the experiment were manufactured by Vietnam Fiber Reinforced Polymer Products, JSC. The average tensile strength and tensile modulus of elasticity of GFRP bars are 970 MPa and 44300 MPa respectively [14]. The deformed steel bars have average yield strength σ_y of 412 MPa, ultimate tensile strength σ_u of 577 MPa and modulus of elasticity E_s=200 GPa. Modulus of elasticity E_b, prismatic strength R_b and tensile strength R_{bt} of concrete are determined empirically through the cubic strength: R_b=0.8R_m; R_{bt}=5R_m/(45+R_m), MPa and E_b=55000R_m/(27+R_m), MPa [15]. The experimental tensile stress-strain relationships of steel and GFRP bar are illustrated in Figure 4.

2.2. Test Setup and Instrumentation

All beams were tested up to failure under a monotonic load in four-point bending test as shown in Figure 2. One LVDT that measures the midspan deflection was placed in the midspan, and two dial indicators I1 and I2 were placed at both ends of the beam to eliminate holder deformation. Load on beams from hydraulic jack is recorded by a 300 kN loadcell. Data from LVDT and loadcell are collected by Wireless Wi-Fi Data Logger STS-WIFI. Data from dual indicators are collected with naked eyes.

Before loading on beam, a 2 kN preloading step was performed to check and eliminate the errors of the instruments at the initial stage of loading. The load applied on beam was gradually increased by steps. The rate of the actuator was set to 3 kN/min. during load control and 2 mm/min. during displacement control. At each level of loading, the load was held constant for approximately 10-15 seconds for recording data from dual indicators and drawing crack patterns. The propagation of cracks was marked by a color marker directly on each beam.

3. Test results and Discussion

3.1. Analysis of Behavior Stages and Failure Process

The load-deflection curves of all tested hybrid GFRP/steel RC beams (Figure 5) show that the behavior of hybrid GFRP/steel RC beams from start of loading until complete failure could be divided into three stages or four stages depending on reinforcement ratios and configurations: first stage - pre-cracking stage (elastic stage); second stage - after concrete cracking and before steel yielding; third stage - post-yield stage of the steel bar until peak load and fourth stage – failure stage (after peak load).

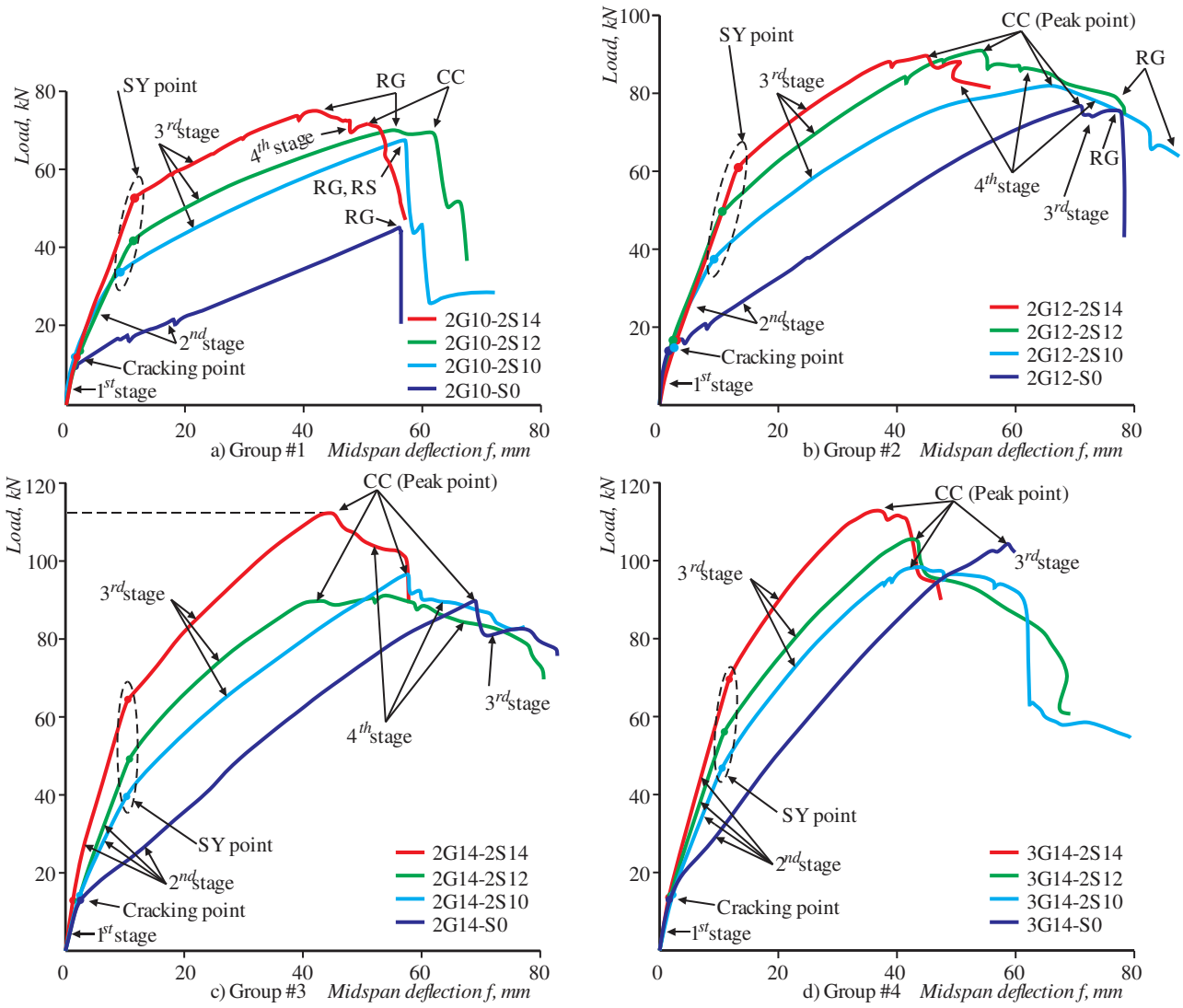

Notes: SY – steel yielding; RG - rupture of GFRP; RS - rupture of steel; CC - concrete crushing

Figure 5. Load-deflection curves of tested beams

In the first stage, the materials behave elastically, so load-deflection relationships of tested beams are linear. At the end of this stage, the deflections of the tested beam vary from 1.53 mm to 2.63 mm, which are 1.91-5.09% of deflections at peak point (Table 2). After concrete cracked, the stiffness of the beams decreases, deflections rapidly increase. This is shown by the decrease of the slopes on load-deflection curves. In this second stage, the load-deflection relationship is approximately linear, so the stiffness of tested beams in this stage is nearly stable. At the steel yielding point, the deflections of tested beams vary from 8.9 mm to 12.7 mm (Table 2), which are about 13.5-31.15% of deflections at peak point. In the third stage, after the steel bar yielded, the stiffness of the hybrid RC beam is further reduced, and the midspan deflection rises rapidly. It can be seen on Figure 5 that at this stage the load-deflection relationships of tested beams are almost linear, so the stiffness of hybrid RC beams in this stage also remains stable. At the end of the third stage, if one of the strains in the GFRP bar or in the outmost compressive concrete fiber reaches its limit value, the beam will be collapsed. It is noted that the rupture strain of steel bar is much higher than that of GFRP, so the rupture of GFRP occurs before the rupture of steel bar. In hybrid RC beams with low GFRP and steel reinforcement ratios (with lack of reinforcements), at the end of the third stage, strain of GFRP bar

reaches the limit value. Once the GFRP has failed, the tensile stress of steel bars would immediately surpass the ultimate stress value then the beams would breakdown without any forewarning (beam 2G10-2S10). In this case, the behavior of hybrid RC beam undergoes only the first three stages. For the beams with high GFRP and steel reinforcement ratios, after the third stage (at the peak load) the beam will be damaged by rupture of GFRP or crushing of concrete in the compression zone (beams 2G10-2S14 and 2G12-2S14). After that the load will decrease gradually and the deflection will increase rapidly. In this case, after peak load, the beams are still able to remain a part of applying load, and the behavior of the hybrid RC beams is divided into four stages. The fourth stage is characterized by the descending branch of load-deflection curves.

Table 2. Testing results

Group of beams	Beam ID	Failure mode	Cracking point		Yielding point			Peak point			Ultimate point
			P_{cr}, kN	f_{cr}, mm	P_y, kN	M_y, kNm	f_y, mm	P_p, kN	M_u, kNm	f_p, mm	f_u, mm
#1 (2G10)	2G10-S0	RG	10.6	1.93	-	-	-	46.0	23.0	56.53	56.53
	2G10-2S10	SY-RG and RS	12.4	1.38	31.4	15.7	8.92	68.7	34.4	57.54	56.53
	2G10-2S12	SY-RG and CC	13.9	2.39	42.2	21.1	11.21	71.0	35.5	55.49	68.00
	2G10-2S14	SY-RG and CC	12.4	1.80	52.3	26.2	11.20	75.9	38.0	42.09	54.87
#2 (2G12)	2G12-S0	CC	13.1	1.85	-	-	-	77.1	38.6	70.95	78.39
	2G12-2S10	SY-CC	11.6	1.26	35.2	17.6	8.90	82.5	41.3	65.98	83.19
	2G12-2S12	SY-CC	14.4	1.72	49.7	24.9	10.53	91.2	45.6	53.90	78.15
	2G12-2S14	SY-CC	13.0	2.08	58.4	29.2	12.70	89.9	45.0	44.85	55.92
#3 (2G14)	2G14-S0	CC	13.0	2.53	-	-	-	90.1	45.1	69.04	82.87
	2G14-2S10	SY-CC	14.2	2.40	39.7	19.8	10.28	96.8	48.4	57.57	75.61
	2G14-2S12	SY-CC	12.7	2.10	49.2	24.6	10.74	91.5	45.8	42.20	78.59
	2G14-2S14	SY-CC	13.0	1.26	64.5	32.3	10.50	113.0	56.5	44.42	59.28
#4 (3G14)	3G14-S0	CC	13.3	1.81	-	-	-	104.7	52.4	58.69	59.92
	3G14-2S10	SY-CC	14.3	2.22	46.8	23.4	10.49	98.8	49.4	43.60	62.75
	3G14-2S12	SY-CC	14.1	1.89	56.1	28.1	10.88	106.1	53.1	42.43	56.67
	3G14-2S14	SY-CC	13.6	1.55	69.0	34.5	11.56	113.4	56.7	37.11	43.75

Note: P_{cr} and f_{cr} are the load and deflection at cracking point respectively; P_y and f_y are the load and deflection at steel yielding point respectively; P_p and f_p are the load and deflection at peak point respectively; f_u is the deflection at ultimate point, which is equal to 85% of the peak load on the descending branch; M_y and M_u – the steel yielding moment and moment-carrying capacity of the beams (M_y=P_y×1 m/2 and M_u=P_p×1 m/2).

Similar analysis of the GFRP RC beams indicates that the beams undergo only two stages (pre-cracking and after concrete cracking – beam 2G10-S0) or three stages (pre-cracking, after concrete cracking and failure – beams 2G12-S0; 2G14-S0 and 3G14-S0).

Depending on reinforcement configuration and the ratio of reinforcements ρ_g, the failure modes of hybrid GFRP/steel RC beams vary. Some of the failure modes of hybrid GFRP/steel RC beams were reported in the previous studies. Based on the above-analyzed experimental results and results published in literature, the following six failure modes of hybrid GFRP/steel can be drawn. Mode 1- steel yielding, GFRP rupturing and then steel rupturing immediately, concrete non-crushing (beam 2G10-2S10). This is a brittle failure that is similar to the under-reinforced concrete beams. This failure mode is also mentioned in [5, 16, 17]. When the strain of GFRP rebars reaches the ultimate value, the steel rebars have already yielded as their yielding strain is smaller than the ultimate strain of the GFRP. This mode is a brittle failure and is therefore not suggested in practice. Mode 2 - steel yielding, GFRP rupturing and sequentially concrete crushing (beams 2G10-2S12 and 2G10-2S14). In this case, first, steel yields and then GFRP ruptures, which involve the crush of concrete in compression zone. The breakdown of beams occurs without rupture of steel bars. Mode 3 - steel yielding, concrete crushing, FRP non-rupturing. This failure mode occurs in the remaining tested hybrid RC beams and also reported in [5, 6, 9, 17, 18]. Mode 4 - concrete crushing without yielding of steel as reported in [5, 6, 9, 16, 17, 18]. This failure mode may occur if the hybrid member reinforced with too much reinforcement and is not allowed in practical structure for its brittle failure. Mode 5 - steel yielding, rupture of GFRP and concrete crushing simultaneously (balanced reinforced) as recorded in [11]. Mode 6 - steel yielding and concrete crushing simultaneously (balanced reinforced) [11]. The failure modes of tested GFRP RC beams are rupture of GFRP (beam 2G10-S0) and crush of concrete (beams 2G12-S0; 2G14-S0 and 3G14-S0). Details of failure modes of tested beams obtained from experiment are shown in Table 2 and Figure 6.

3.2. Analysis of Crack Patterns at Failure

Crack patterns of the tested beams were observed and redrawn after each step of loading. After concrete cracking, the number of cracks in hybrid RC beams developed. After yielding of steel the existing cracks propagate until the beam is broken and almost no new cracks appear. Crack patterns after failure of tested beams are illustrated in Figure 6. The overall distribution of the cracks is relatively uniform and symmetric over a length of 1700 mm to 1980 mm in the middle of the beams. The numbers of minor and major cracks and the average minor and major crack spacing of tested beams at failure are shown on Figure 7. Testing results show that when increasing the total reinforcement ratio, i.e. increasing the number of longitudinal bars, the number of major and minor cracks expands, the crack distribution length enhances, the average minor and major crack spacing reduce. This phenomenon is explained by higher bond strength when increasing the number of longitudinal bars. These experimental results are consistent with the results of previous studies. Aiello and Ombres [19] tested hybrid GFRP/steel RC beams with span 2700 mm, pure bending zone 100 mm and reported that at failure the major crack spacing was about from 60 mm to 100 mm and the number of cracks was from 25 to 30. The study results of Ge W. et al. [18] indicated that the average crack spacing of hybrid BFRP/steel RC beams at failure was from 93 mm to 108 mm.

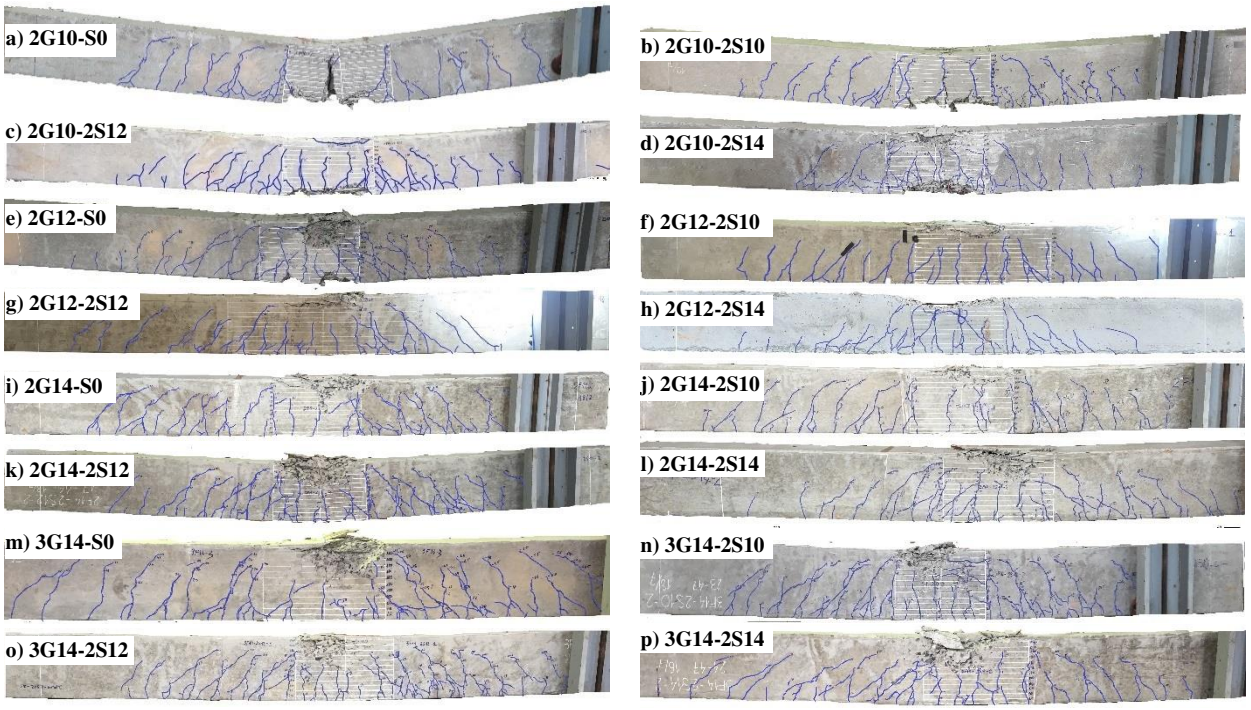

Figure 6. Crack patterns and failure modes of tested beams

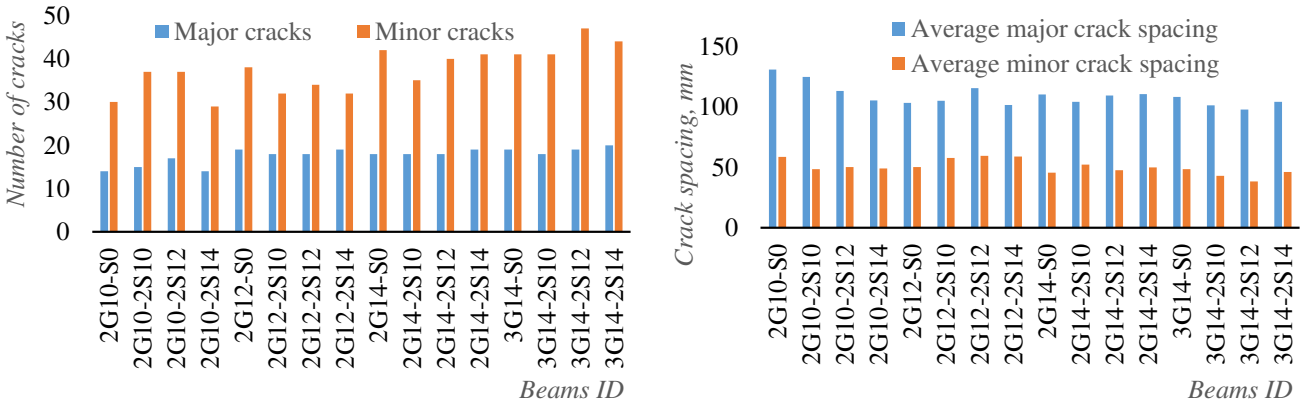

a) Number of cracks b) Average crack spacing

Figure 7. Number of cracks and average crack spacing at failure

3.3. Analysis of Secondary Stiffness and Ductility Index

Figure 8 shows the schematic diagrams for determining the stiffness and ductility of tested hybrid RC beams based

on the experimental load-deflection curve. In this study, initial equivalent stiffness K_i (before steel yielding) and secondary stiffness K_{III} (after steel yielding) of hybrid GFRP/steel RC beams were calculated and analyzed. These stiffnesses can be defined as follows [12]:

$$K_i = P_y/f_y \quad (1)$$

$$K_{III} = \frac{P_P - P_y}{f_P - f_y} \quad (2)$$

Where: P_y, f_y, and P_p, f_p are listed in Table 2.

Secondary stiffness ratio of the tested hybrid RC beams is calculated by following equation:

$$r_b = K_{III}/K_i \quad (3)$$

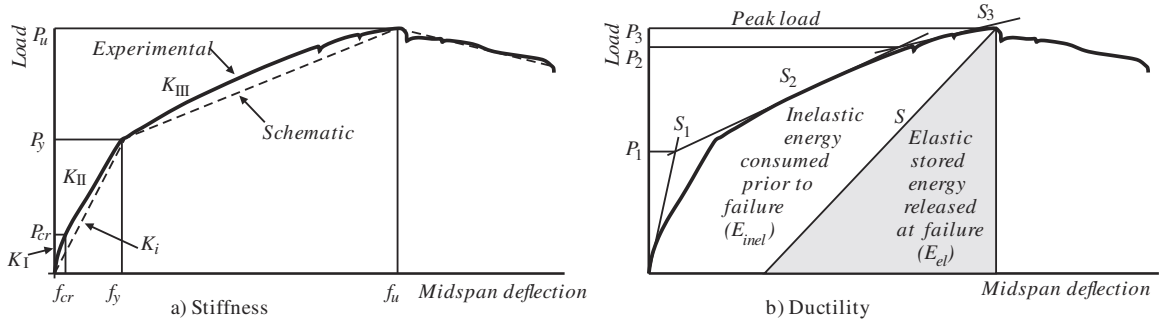

Figure 8. Diagrams of stiffness and ductility indexes

Flexural stiffness of RC beams depends mainly on their cross-sectional area and modulus of elasticity of materials. The calculated results in Table 3 and Figure 9 show that in each group of hybrid RC beams with fixing GFRP reinforcement, the initial stiffness of tested beams increases proportionally to the increase in the ratio of steel reinforcement. Similarly, when steel reinforcement is fixed, the initial stiffness of hybrid RC beams also ascends linearly with the GFRP reinforcement ratio. For groups of hybrid RC beams with fixing GFRP reinforcement (Figure 9a and Table 3), when increasing steel reinforcement ratios from 0.51% to about 1.1% the initial equivalent stiffness of groups of beams 2G10, 2G12, 2G14 and 3G14 increases 1.33, 1.22, 1.59 and 1.34 times respectively. In groups of beams with fixing steel reinforcement 2S10, 2S12 and 2S14 (Figure 9b and Table 3), when increasing GFRP reinforcement ratios from 0.35% to 1.19%, the initial stiffness increases 1.27, 1.37 and 1.28 times respectively. These results indicate that in hybrid RC beams influence of steel reinforcement on the initial equivalent stiffness is greater than the effect of GFRP due to the important difference in elastic modulus.

Development of cracks and yielding of steel lead to significant loss of secondary stiffness. The results in Table 3 show that after yielding of steel the secondary stiffness of hybrid RC beams in each group of tested hybrid beams with fixing GFRP reinforcement is almost the same despite steel reinforcement varies, and the average values of stiffness of these groups rise along with the increase of GFRP reinforcement. This outcome indicates that the influence of steel reinforcement after yielding on the stiffness of hybrid RC beams is negligible. Specifically, after steel yielding the stiffness of hybrid RC beams reduces by 65-84% in comparison with the initial stiffness. Secondary stiffness ratio r_b shows the reducing ratio of stiffness after steel yielding to the initial stiffness. For the tested hybrid RC beams, the stiffness ratios vary from 0.16 to 0.35 depending on reinforcement ratio and the secondary stiffness ratio is inversely proportional to the steel reinforcement ratio in each group. As mentioned above, the steel reinforcement significantly influences the stiffness of hybrid RC beams, thus the secondary stiffness ratio increases with the increase of the ratio of reinforcements ρ_g (Figure 10).

Table 3. Stiffness, ductility and toughness of tested beams

Group of beams	Beam ID	Reinforcement ratio				Stiffness			Ductility						Toughness
		μ_s, %	μ_g, %	μ_b, %	ρ_g	K_i, kN/mm	K_{III}, kN/mm	r_b	E_{el}, kNmm	E_{inel}, kNmm	E_{inel}/E_{tot}, %	Classification	μ_Δ	μ	$U_{T,p}$, MPa
#1 (2G10)	2G10-S0	-	0.36	0.36	-	-	-	-	303.9	1284.1	80.9	Ductile	1.00	3.11	17.3
	2G10-2S10	0.52	0.36	0.88	0.71	3.52	0.77	0.22	440.0	2357.0	84.3	Ductile	6.34	3.68	30.2
	2G10-2S12	0.76	0.35	1.11	0.48	3.76	0.65	0.17	472.9	2459.1	83.9	Ductile	6.07	3.60	31.4
	2G10-2S14	1.07	0.37	1.44	0.35	4.67	0.76	0.16	331.0	2027.0	86.0	Ductile	4.90	4.06	25.9
#2 (2G12)	2G12-S0	-	0.55	0.55	-	-	-	-	734.2	3220.8	81.4	Ductile	1.10	3.19	43.8
	2G12-2S10	0.54	0.57	1.11	1.06	3.95	0.83	0.21	706.7	3262.3	82.2	Ductile	9.35	3.31	44.1
	2G12-2S12	0.73	0.54	1.27	0.74	4.72	0.96	0.20	632.7	2935.3	82.3	Ductile	7.42	3.32	38.1
	2G12-2S14	1.10	0.57	1.67	0.52	4.60	0.90	0.19	459.8	2471.2	84.3	Ductile	4.40	3.69	32.6

#3 (2G14)	2G14-S0	-	0.81	0.81	-	-	-	-	1628.6	3182.8	66.2	Brittle	1.20	1.98	52.2
	2G14-2S10	0.52	0.80	1.32	1.54	3.86	1.21	0.31	1200.3	2425.7	66.9	Less ductile	7.36	2.01	39.9
	2G14-2S12	0.78	0.79	1.57	1.01	4.58	1.34	0.29	940.9	2696.1	74.1	Less ductile	7.32	2.43	41.0
	2G14-2S14	1.06	0.79	1.85	0.75	6.14	1.43	0.23	931.2	2578.8	73.5	Less ductile	5.65	2.38	37.9
#4 (3G14)	3G14-S0	-	1.17	1.17	-	-	-	-	1737.6	2152.4	55.3	Brittle	1.02	1.62	41.7
	3G14-2S10	0.51	1.19	1.70	2.33	4.46	1.57	0.35	1189.1	1667.9	58.4	Brittle	5.98	1.70	30.8
	3G14-2S12	0.74	1.16	1.90	1.57	5.16	1.58	0.31	1100.4	1935.6	63.8	Brittle	5.21	1.88	32.5
	3G14-2S14	1.01	1.11	2.12	1.10	5.97	1.74	0.29	1000.3	1876.7	65.2	Brittle	3.78	1.94	30.3

The ductility of the structure mentions as the inelastic deformation capacity prior to collapse without significant loss of strength. The greater the ductility, the greater the ultimate deformation capacity, and the structure will be relatively safer under the same load. It is well-known that the ductility of reinforced concrete beams is directly related to the amount of tension reinforcement. A higher tensile reinforcement ratio results in less ductile behavior. The ductility can be expressed in terms of displacement or energy absorption. The displacement ductility can be obtained from the ratio of ultimate displacement to the yield displacement. The energy ductility can be defined as the ratio relating any two of the inelastic, elastic energies to total energy (Figure 8b). The conventional ductility or displacement ductility cannot be applied to hybrid RC beams, because it does not include the effect of the secondary stiffness, which leads to increase the ductility of hybrid RC beams [7, 12]. Therefore, in this paper the energy ductility index μ of tested beams is calculated and analyzed. In addition, as a basis for comparison, the displacement ductility is also calculated (Table 3).

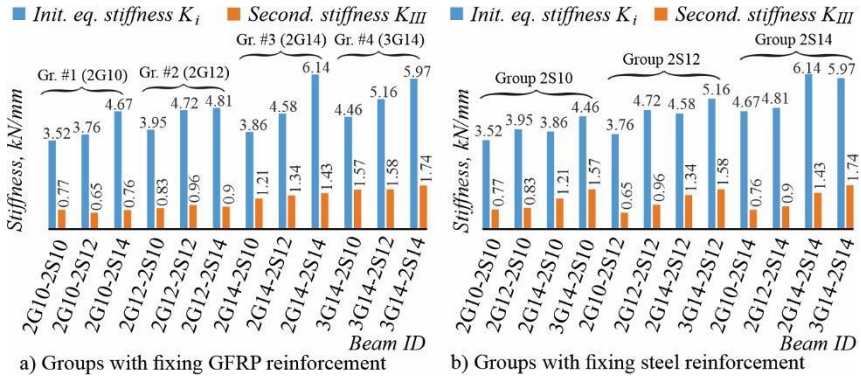

Figure 9. Initial equivalent stiffness and secondary stiffness of hybrid GFRP/steel RC beams

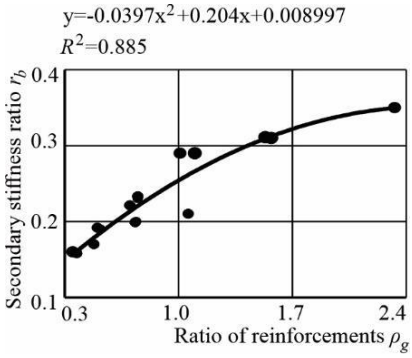

Figure 10. Secondary stiffness ratio versus ratio of reinforcements

According to Figure 8b, the slope of the line separating the elastic energy from the inelastic energy can be obtained as follows [20]:

$$S = \frac{P_1 S_1 + (P_2 - P_1) S_2}{P_2} \tag{4}$$

Where: P_1 and P_2 – loads as shown in Figure 8b, S_1 and S_2 – corresponding slopes.

Total energy:

$$E_{tot} = E_{inel} + E_{el} \tag{5}$$

The energy ductility index can be calculated as follows [21] and the results are shown in Table 3:

$$\mu = \frac{1}{2}\left(\frac{E_{tot}}{E_{el}} + 1\right) \tag{6}$$

The calculated results of energy ductility indexes in Table 3 and on Figure 11a indicate that in each group of beams with fixing the GFRP reinforcement, the ductility indexes of hybrid GFRP/steel RC beams increase with boost of the steel reinforcement ratio and these relationships follow a linear trend. The GFRP reinforcement ratio versus ductility index relationships of these groups is illustrated in Figure 11b. It can be seen that an increase in GFRP ratio reduces the ductility index of tested beam and these relationships also have linear tendency.

The ductility of RC beams relates to the shape of the load-displacement relationship of the sections, which is mainly decided by the ratio of steel reinforcement to GFRP reinforcement and total reinforcement. From Table 3 and Figure 11c it can be seen that the ductility indexes of hybrid RC beams are inversely related to the ratio of

reinforcement ρ_g. Simultaneously, with the same ratio ρ_g the ductility index is inversely proportional to the total reinforcement ratio. For example, beams 2G10-2S10, 2G12-2S12 and 2G14-2S14 have nearly the same values of ratio ρ_g when total reinforcement ratios vary from 0.87% to 1.85% (ratio 1:1.46:2.12), the ductility indexes reduce from 3.68 to 2.38 (ratio 1:0.9:0.65). Similarly, the above finding can be verified with pairs of beams 2G12-2S10 and 2G14-2S12 or 2G14-2S10 and 3G14-2S12. When increasing the steel reinforcement ratios from 0% to about 1.1%, the ductility indexes of groups of hybrid RC beams reinforced with 2G10, 2G12, 2G14 and 3G14 increase by 1.31, 1.16, 1.2 and 1.2 times. For groups of beams with fixing steel reinforcement (Group S0 - without steel reinforcement, group 2S10, group 2S12 and group 2S14), when GFRP reinforcement ratios increase from 0.36% to 1.19%, the ductility indexes decrease respectively 1.92, 2.16, 1.91 and 2.09 times.

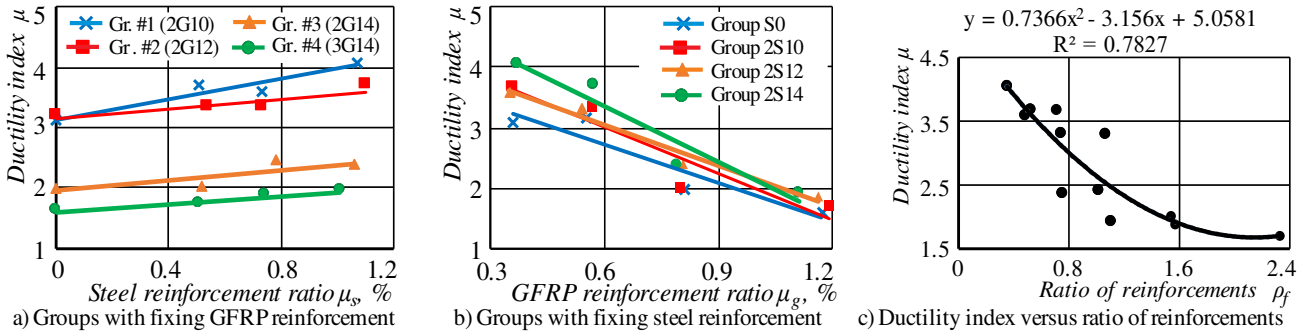

a) Groups with fixing GFRP reinforcement b) Groups with fixing steel reinforcement c) Ductility index versus ratio of reinforcements

Figure 11. Energy ductility indexes of tested beams

With the purpose to classify the tested beams according to their ductility, the energy ratio is defined as the ratio of the inelastic energy to total energy (E_{inel}/E_{tot}). In the light of this study, if the displacement ductility requirement of energy ductility index is greater than 3 or corresponding energy ratio E_{inel}/E_{tot} is more than 80%, the authors suggest that the hybrid beams will exhibit a ductile failure. On the other hand, when the energy ductility index ranges between 2 and 3, the beams will be considered to be less ductile behavior. In another case, the beam experiences a brittle failure if the energy ratio is below 65% or energy ductility index is less than 2. Ductility classification of the tested beams according to their ductility is listed in Table 3. Table 3 depicts that all beams of group #1 and #2 except for the beams 2G10-S0 and 2G12-S0, present not only the energy ductility index greater than 3 but also present E_{inel}/E_{tot} ratio greater than 80%. In this case, two beams of 2G10-S0 and 2G12-S0 indicate that the inelastic energies consumed prior to failure, E_{inel} accounts for more than 80% of total energies but the displacement ductility μ_Δ is even equal to 1.0 and 1.10, respectively. This finding is in agreement with Maranan et al.'s data [8]. It can be seen that for groups of beams #3 and #4, whose amount of GFRP ratios are nearly twice and three times higher than the balanced GFRP ratio, the E_{inel}/E_{tot} ratios have dropped considerably by 30% and 40% respectively in comparison with groups of beams #1 or #2. It is obvious that the high GFRP ratios in hybrid beams reduce considerably the energy dissipation capacity after yielding of hybrid beams.

3.4. Analysis of Toughness

The toughness U_T is the ability of a material to absorb energy and plastically deform without fracturing [22]. This parameter can be calculated by dividing total area below the stress–strain curve or the force–deformation curve by the volume of the tested beam. In this work, the force–deformation curves are used for determining the toughness at peak load ($U_{T,p}$). The calculated values of toughness of tested beams are listed in Table 3 and compared on Figure 12 for each group of beams.

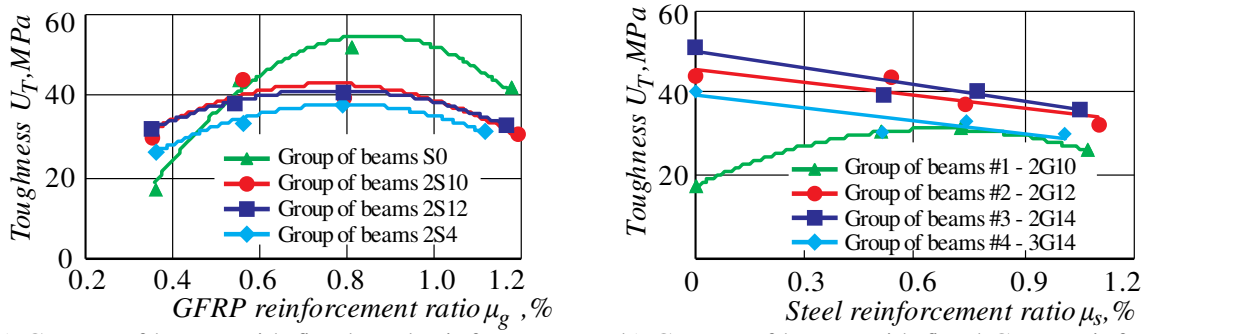

a) Groups of beams with fixed steel reinforcement b) Groups of beams with fixed GFRP reinforcement

Figure 12. Toughness of tested beams

It can be seen in Figure 12a, in group with fixing the steel reinforcement, the toughnesses of GFRP RC and hybrid RC beams at peak point increase when increasing the GFRP reinforcement ratio to 0.8%. Further increasing GFRP

reinforcement ratio will lead to a reduction in this toughness. In groups of beams with fixing GFRP reinforcement (Figure 12b), the changing tendency of toughness at peak point is various. In the group of beams #1 (2G10), the toughness at peak point and ultimate point enhances when increasing steel reinforcement ratio to 0.6%. After that the toughness at peak point tends to decrease when the steel reinforcement ratio increases from 0.6 to 1.1% (Figure 12b). Meanwhile, for groups of beams #2 (2G12), #3 (2G14) and #4 (3G14), the toughness at peak point tends to decrease with the increase of steel reinforcement ratio. Moreover, the toughness of groups #4 at ultimate point is around 35% lower than that of groups #3 since the GFRP ratio is approximately three times higher than the balanced GFRP ratio. The reason is that increasing steel reinforcement in groups of beams #2 (2G12), #3 (2G14) and #4 (3G14) reduces significantly deflections at peak point, meanwhile, the peak loads of the beams in each of these groups vary insignificantly due to failure by crush of concrete in the compression zone.

3.5. Analysis of Steel Yielding Moment and Moment-carrying Capacity

The steel yielding load listed in Table 2 is determined by the load at the point of sudden change in deflection on load-displacement curve (Figure 5). To clarify the effect of GFRP reinforcement on steel yielding moment (M_y) in each group of beams, the steel yielding moment evolution as a function of the GFRP reinforcement ratio was build and shown in Figure 13. Before yielding of steel, the GFRP and steel reinforcements receive the tensile force. So, increasing GFRP reinforcement ratio boosts steel yielding load and the GFRP reinforcement ratio versus steel yielding moment relationships are linear (Figure 13). At the same time, GFRP reinforcement ratio-steel yielding moment relationships of all groups of beams with fixing steel reinforcement ratio have the same tendency. Specifically, when increasing GFRP reinforcement ratio from 0.35% to 1.19%, the steel yielding moment of groups 2S10, 2S12 and 2S14 enhances 1.37, 1.33 and 1.32 times, respectively.

Observing the load-deflections in Figure 5, after steel yielding, due to the large ultimate train of GFRP the hybrid RC beams continues to receive the load. The load gain carried by the hybrid RC beams between the steel yielding point and the peak point depends mainly on the steel reinforcement ratio, GFRP reinforcement ratio and concrete strength. According to the experimental results in Table 3, with the same GFRP reinforcement ratio, the load gain between the steel yielding point and peak point of hybrid RC beams reduces when increasing steel reinforcement ratio. On the contrary when fixing steel reinforcement load gain increases proportionally to GFRP reinforcement ratio.

The experimental load-carrying capacity of the tested beams listed in Table 2 is determined at the peak point of load-displacement curve (Figure 5). The moment-carrying capacity (M_u) versus reinforcement ratio relationships for all tested beams is illustrated in Figure 14. In group with fixing steel reinforcement (groups S0; 2S10; 2S12 and 2S14), as the GFRP reinforcement ratio increases from 0.35% to 1.2%, the moment bearing capacity of GFRP RC beams (Group S0) rise to 128.1%, the corresponding values for groups of beams 2S10, 2S12 and 2S14 are 43.8%, 49.4% and 49.4% respectively (Figure 14a). Besides, the Figure 14a shows that the load-carrying capacity of groups of beams with fixing steel reinforcement sharply increases in range of GFRP reinforcement from 0.35% to 0.8%. After that the difference of load-carrying capacities of tested beams is not significant when further increasing GFRP reinforcement ratio (Figure 14a). This can be explained by the failure initiated at concrete compression zone. At GFRP reinforcement ratio about 1.2%, the difference of moment-carrying capacities of tested beams is not significant.

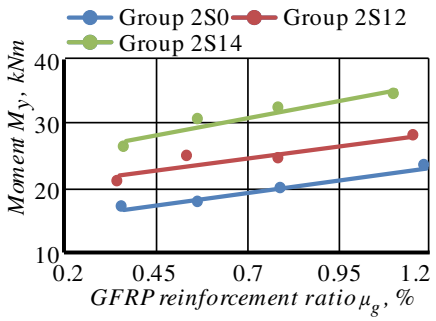

Figure 13. Relationship between GFRP reinforcement ratio and steel yielding load

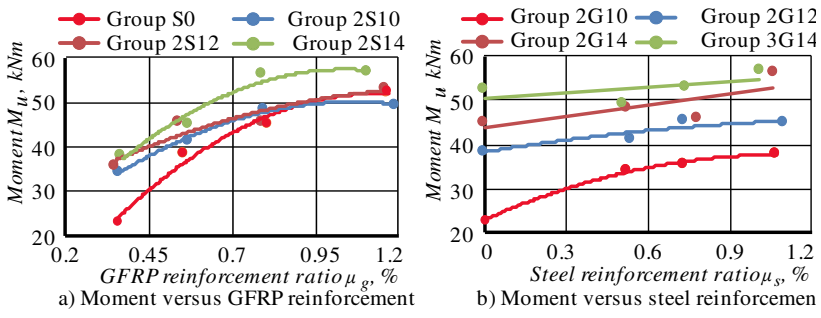

Figure 14. Moment-carrying capacity versus reinforcement ratio relationships

To evaluate the effect of steel reinforcement on the moment-carrying capacity of hybrid RC beams, the moment-carrying capacity versus steel reinforcement ratio relationships were presented in Figure 14b. It can be seen on Figure 14b that influence of steel reinforcement on load-carrying capacity of hybrid RC beams is dissimilar. When adding steel reinforcement with the ratio from 0% to 1.07% to GFRP under-reinforced concrete beam 2G10, the moment-carrying capacity increases to 65.4%. Meanwhile, adding steel reinforcement from 0% to about 1.07% to the GFRP over-reinforced beams (2G12, 2G14 and 3G14) leads to an increase in moment-carrying capacity of 16.6%, 25.4 and

8.3%, respectively. With the same total reinforcement ratio, the load-carrying capacity of the hybrid RC beams increase when increasing the ratio ρ_g (for example, the beams 2G10-2S12, 2G12-2S10 and 3G14-S0 or the beams 2G12-2S14, 3G14-2S10).

Depending on the reinforcement configuration, the ratio of the steel yielding moment to moment capacity of the tested beams (M_y/M_u) varies from 0.41 to 0.69. In each group of beams with fixing GFRP reinforcement ratio the ratios of M_y/M_u improve when increasing steel reinforcement ratio. It is noticed from experimental results that with the same total reinforcement ratio, the steel yielding moment is proportional to the ratio ρ_g (pairs of beams: 2G10-2S12 versus 2G12-2S; 2G12-2S14 versus 3G14-2S10; 2G14-2S14 versus 3G14-2S12 etc.).

4. Predicted Model of Moment-carrying Capacity and Steel Yielding Moment

As stated above, several methods of calculating the bearing capacity of beams of hybrid FRP/steel have been proposed by some authors in previous studies. Recently, Kara et al. [9] classified three failure modes and proposed the formulas to predict the flexural capacity for hybrid FRP/steel RC beams based on equilibrium of forces and full compatibility of strains. It was reported that the ratio of predicted value to experimental value of flexural capacity varied in wide range (between 0.77 and 1.25). The reason is probably because the authors employed the inappropriate stress-strain diagrams of materials. Lei Pang et al. [5] considered the strength at initiation of yielding (M_y) as the design-aimed state and the difference between the flexural strength at the ultimate state and that at the steel yielding state can be considered as the reserve strength. Then, they proposed the formula to predict the steel yielding moment according to the provisions of ACI 318M-05.

In this paper, the authors introduce another method to determine the steel yielding moment and moment-carrying capacity of hybrid GFRP/steel RC beams based on the deformation models of materials [23]. For GFRP bars, according to the tensile test [14], the stress-strain relationship is linear until failure (Figure 4). Tri-linear simplified stress-strain diagram according to SP 63.13330.2018 [23] is chosen for concrete (Figure 15a). The stress-strain relationship of steel bar is also formulated as a simplified trilinear diagram based on the actual relationship (Figure 15b). All characteristic points in Figure 15 are taken from SP 63.13330.2018 [23].

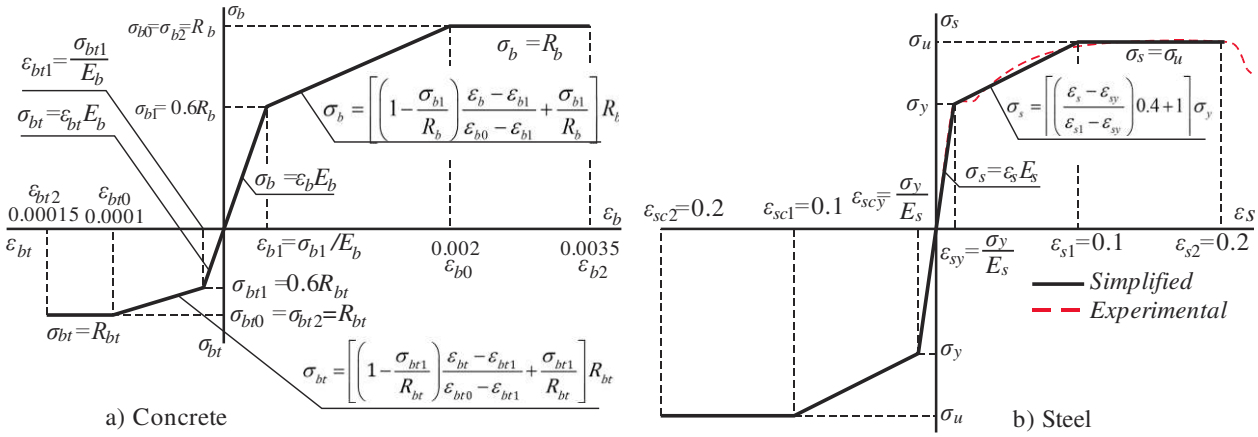

Note: R_b and R_{bt} are the prismatic compressive and tensile strength of concrete respectively; σ_y and σ_u – yield stress and ultimate stress of steel.

Figure 15. Tri-linear simplified stress-strain diagrams of concrete and steel bars

In order to ensure accuracy, in the calculation procedure the compressive reinforcement area (A_{sc}) is taken into account. The normal cross-section is divided to n equal segments (layers) in height (Figure 16). Assuming that: "Plane cross-section remains plane before and after bending"; each fiber works under stress conditions in a single axis of stress state.

In calculation, the forces and deformations in a cross-section are determined according to non-linear deformation models using equilibrium expressions of internal and external forces in the section. In addition, distribution of concrete strain and reinforcement strain along the sectional height is assumed according to the linear law (flat cross-section hypothesis). Regarding the algebraic sign convention, "minus" refers to axial compression force, compressive stresses and strains of concrete and reinforcement; "plus" stands for axial tension force, tensile stresses and elongation strains of concrete and reinforcement.

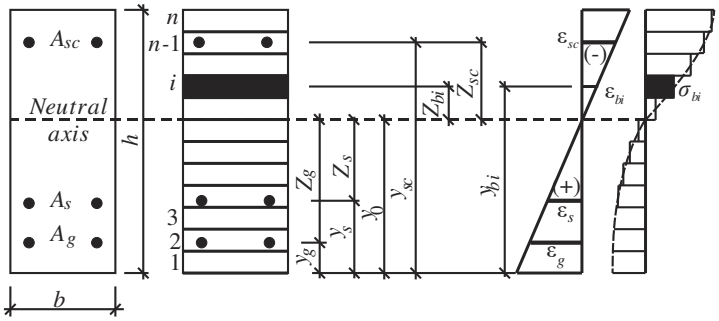

Figure 16. Design scheme of a normal section

For bending element in the symmetrical plane of the normal cross section and the X-axis in this plane, the moment equilibrium is as follows:

$$M = D_{11}(1/r_x) \tag{7}$$

Where: $1/r_x$ - the curvature of element and D_{11} - rigidity characteristic of cross section. The values of these parameters are determined as in following equations:

$$1/r_x = \varepsilon_{bi}/Z_{bi} = \varepsilon_s/Z_s = \varepsilon_{sc}/Z_{sc} = \varepsilon_g/Z_g \tag{8}$$

$$D_{11} = \sum_{i=1\ldots n} A_{bi}Z_{bi}^2E_b\nu_{bi} + A_sZ_s^2E_s\nu_s + A_{sc}Z_{sc}^2E_s\nu_{sc} + A_gZ_g^2E_g \tag{9}$$

Where: ε_{bi}, ε_s, ε_{sc}, ε_g, Z_{bi}, Z_s, Z_{sc}, Z_g shown in Figure 16; E_b, E_s and E_g – the modulus's of elasticity of concrete, steel in tension zone, steel in compression zone and GFRP respectively; ν_{bi}, ν_s and ν_{sc} - elastic coefficients of concrete in *i*-layer, steel in tension zone and compression zone, respectively. These values are determined by following formulas:

$$\nu_{bi} = \frac{\sigma_{bi}}{E_b\varepsilon_{bi}} \text{ (Note: if } \varepsilon_{bi}>0\text{, i.e. tensile strain, use } \sigma_{bti} \text{ instead of } \sigma_{bi}) \tag{10}$$

$$\nu_s = \frac{\sigma_s}{E_s\varepsilon_s} \tag{11}$$

$$\nu_{sc} = \frac{\sigma_{sc}}{E_s\varepsilon_{sc}} \tag{12}$$

Where: σ_{bi} (σ_{bti}), σ_s and σ_{sc} – stress in *i*-layer of concrete, in steels in tension zone and compression zone respectively.

Strain of materials are determined from the equilibrium of cross section as follows:

$$\varepsilon_{bi} = MZ_{bi} / D_{11} \text{ (where } Z_{bi} = y_0 - y_{bi}) \tag{13}$$

$$\varepsilon_g = MZ_g / D_{11} \text{ (where } Z_g = y_0 - y_g) \tag{14}$$

$$\varepsilon_s = MZ_s / D_{11} \text{ (where } Z_s = y_0 - y_s) \tag{15}$$

$$\varepsilon_{sc} = MZ_{sc} / D_{11} \text{ (where } Z_{sc} = y_0 - y_{sc}) \tag{16}$$

Coordinate of neutral axis of cross section y_0:

$$y_0 = \frac{\sum_{i=1\ldots n} A_{bi}y_{bi}E_b\nu_{bi} + A_sy_sE_s\nu_s + A_{sc}y_{sc}E_{sc}\nu_{sc} + A_gy_gE_g}{D_{33}} \tag{17}$$

Rigidity characteristic of cross section D_{33} is defined as follows:

$$D_{33} = \sum_i A_{bi}E_b\nu_{bi} + A_sE_s\nu_s + A_{sc}E_{sc}\nu_{sc} + A_gE_g \tag{18}$$

Steel yielding condition:

$$\varepsilon_s = \varepsilon_{s,y} \tag{19}$$

Where: $\varepsilon_{s,y}=\sigma_{s,y}/E_s$ - strain of steel at yield point.

The reinforced concrete beam collapses when one of the following conditions is met:

$$\left|\varepsilon_{b,\max}\right| \geq \varepsilon_{b,ult} \tag{20}$$

$$\varepsilon_{s,\max} \geq \varepsilon_{s,ult} \tag{21}$$

$$\varepsilon_{g,\max} \geq \varepsilon_{g,ult} \tag{22}$$

Where: $\varepsilon_{b,max}$ - strain of the most compressive concrete fibre in the normal section due to external load; $\varepsilon_{s,max}$ and $\varepsilon_{g,max}$ - strain of the most tensile steel and GFRP rebars respectively in the normal section due to external load; $\varepsilon_{b,ult}=\varepsilon_{b2}=0.0035$ (Figure 15a) - ultimate strain of compressive concrete assumed in accordance to SP 63.13330.2018 [23]; $\varepsilon_{s,ult}=\varepsilon_{s2}=0.2$ - ultimate strain of steel reinforcement (Figure 15b); $\varepsilon_{g,ult}$ - ultimate strains of GFRP reinforcement according to tensile test result [14]: $\varepsilon_{g,ult}=R_g/E_g$ (Figure 4).

Calculation is performed by iteration method. At first iteration, assuming an initial value of moment ΔM and then calculation is carried out with the moment M_1'=ΔM. At this step, assume that the materials exhibit elastic behavior (i.e. $v_{bi}=v_s=v_{sc}=1$), we determine the rigidity characteristic D_{33} (18), neutral axis position y_0 (17) and the rigidity characteristic D_{11} (9). Next, we define strains of materials ε_{bi} (13), ε_g (14), ε_s (15) and ε_{sc} (16). Stresses in concrete layers, tensile and compressive steel bars, GFRP bars (σ_{bi}, σ_s, σ_{sc} and σ_g) are determined by stress-strains diagrams on Figure 12 and Figure 4 according to received strain values of the materials. After that we define the elastic coefficient v_{bi}, v_s and v_{sc} by (10), (11) and (12) for the second iteration.

At the end of first step, from the found stress values of materials the actual moment of this step is calculated:

$$M_1 = \sum_{i=1\ldots n} A_{bi}\sigma_{bi}Z_{bi} + A_s\sigma_s Z_s + A_{sc}\sigma_{sc}Z_{sc} + A_g\sigma_g Z_g \tag{22}$$

In each subsequent step, the calculation is performed with initial moment M_i'=M_{i-1}+ΔM. At each step, the strain values of materials are controlled according to (19), (20), (21) and (22). At n-step the values of strain in tensile steel bar reaches the yielding strain by condition $\varepsilon_s \geq \varepsilon_{s,y}$ for the first time, the steel yielding moment M_y is taken equal the moment value at this step. Iterative process is continued until one of conditions (20), (21) and (22) is met. Here, we determine the failure mode and flexural capacity M_u of the section, which is taken from the value of moment in the previous step. The calculation results of steel yielding moment and flexural capacity of the tested beams and comparison of the experimental and theoretical values of these moments are displayed in Table 4. The ratios of $M_{u,theor}/M_{u,exp}$ range from 0.88 to 1.11 and the ratios of $M_{y,theor}/M_{y,exp}$ vary between 0.86 and 0.95. Overall, the predicted values obtained from the current analysis are in good agreement with the experimental results for both hybrid GFRP/steel reinforced concrete beams and pure GFRP reinforced concrete beams.

To verify the proposed model, the experimental results of the hybrid GFRP/steel RC beams published in the literature [3, 11, 19] are compared to results obtained from proposed model as shown in Table 4. The average value of the ratio $M_{y,theor}/M_{y,exp}$ and $M_{u,theor}/M_{u,exp}$ are 0.93 and 1.01, respectively. These outcomes indicate that the proposed model is sufficiently reliable to estimate load carrying capacity.

Table 4. Results of beam's steel yielding moment, ultimate moments

Reference	Beam ID	*b, mm*	*h, mm*	A_g, cm^2	A_s, cm^2	A_{sc}, cm^2	Experimental results		Theoretical results		Δ_1	Δ_2
							$M_{y,exp}$, kNm	$M_{u,exp}$, kNm	$M_{y,theor.}$, kNm	$M_{u,theor.}$, kNm		
This Study	2G10-S0	151	253	1.23	-	0.57	-	23.0	-	25.6	-	1.11
	2G10-2S10	152	254	1.23	1.57	0.57	15.7	34.4	14.9	34.7	0.95	1.01
	2G10-2S12	155	252	1.23	2.26	0.57	21.1	35.5	19.8	37.8	0.94	1.06
	2G10-2S14	150	253	1.23	3.08	0.57	26.2	38.0	24.6	38.4	0.94	1.01
	2G12-S0	151	249	1.87	-	0.57	-	38.6	-	36.6	-	0.95
	2G12-2S10	150	250	1.87	1.57	0.57	17.6	41.3	16.2	37.8	0.92	0.92
	2G12-2S12	155	250	1.87	2.26	0.57	24.9	45.6	21.5	41.0	0.87	0.9
	2G12-2S14	151	248	1.87	3.08	0.57	29.2	45.0	25.2	40.8	0.86	0.91

	2G14-S0	150	256	2.65	-	0.57	-	45.1	-	39.7	-	0.88
	2G14-2S10	151	251	2.65	1.57	0.57	19.8	48.4	17.6	43.6	0.89	0.90
	2G14-2S12	148	250	2.65	2.26	0.57	24.6	45.8	23.3	48.0	0.95	1.05
	2G14-2S14	153	255	2.65	3.08	0.57	32.3	56.5	27.8	49.5	0.86	0.88
	3G14-S0	148	255	3.97	-	0.57	-	52.4	-	50.4	-	0.96
	3G14-2S10	152	254	3.97	1.57	0.57	23.4	49.4	20.8	49.6	0.89	1.00
	3G14-2S12	153	254	3.97	2.26	0.57	28.1	53.1	25.6	52.8	0.91	1.00
	3G14-2S14	155	255	3.97	3.08	0.57	34.5	56.7	32.4	60.0	0.94	1.06
Aiello, M. and L. Ombres [19]	A1	150	200	0.883	1.00	1.01	-	25.14	-	22.4	-	0.89
	A2	150	200	1.57	1.00	1.01	-	28.41	-	27.9	-	0.98
	A3	150	200	2.36	2.26	1.01	-	35.55	-	35.8	-	1.01
	B2	150	200	0.88	-	1.01	-	20.21	-	19.3	-	0.95
	C1	150	200	0.88	1.00	1.01	-	25.14	-	24.0	-	0.95
Lau, D. and H. Pam [3]*	G0.3-MD1.0-A90	280	380	2.84	9.82	1.01	101.0	147.0	111.0	168.0	1.10	1.14
	G1.0-T0.7-A90	280	380	9.82	6.28	1.01	161.0	261.0	152.0	232.0	0.94	0.89
	G0.6-T1.0-A90	280	380	5.67	9.82	1.01	178.5	229.0	184.0	240.0	1.03	1.05
Ruan, X. et al. [11]*	2G12-2S12	180	300	2.26	2.26	1.01	39.1	57.5	34.2	62.7	0.87	1.09
	2G16-2S12	180	300	4.02	2.26	1.01	44.3	63.3	39.6	79.8	0.89	1.26
	2G12-1S16	180	300	2.26	2.01	1.01	38.2	56.4	32.4	61.2	0.85	1.09
	2G16-1S16	180	300	4.02	2.01	1.01	45.4	66.7	38.4	75.6	0.85	1.13
	2G12-2S12 (D)	180	300	2.26	2.26	1.01	37.7	53.8	31.2	58.8	0.83	1.09

Note: $\Delta_1=M_{y,theor}/M_{y,exp}$, $\Delta_2=M_{u,theor}/M_{u,exp}$; * The values M_y are not reported by authors, these values are determined by load-deflection curves in these literatures.

5. Conclusions

This paper analyzes the influence of reinforcement ratios as well as configurations to the flexural behavior of hybrid GFRP/steel RC beams and GFRP RC beams. The research is carried out with a wide range of steel reinforcement ratio μ_s, GFRP reinforcement ratio μ_g and ratio of reinforcements ρ_g. From the study results, the following conclusions can be drawn:

- There are four stages of behavior and six failure modes of hybrid GFRP/steel RC beams depending on the longitudinal reinforcement ratios. The findings make a contribution to the existing literature that presented only three stages of behavior and four failure modes of hybrid FRP/steel RC beams;
- The crack patterns, stiffness, ductility and toughness are considerably influenced by the percentage of longitudinal reinforcements μ_s, μ_g and the ratio of longitudinal reinforcements ρ_g;
- It is better to use the energy ductility index to access the ductility of hybrid GFRP/steel RC beams. Using other approaches may lead to significant deviations. Based on the energy ductility index and energy ratio, the failure of hybrid GFRP/steel RC beams can be classified as ductile, less ductile and brittle
- The presence of GFRP reinforcement delays the steel yielding of hybrid RC beams, and the relationship between GFRP reinforcement ratio and steel yielding load is linear. At the same total reinforcement ratio, the load-carrying capacity of hybrid RC beams is improved when increasing the ratio of reinforcement, ρ_g.
- The proposed analytical model using non-linear deformation models of materials can properly predict the steel yielding moment and ultimate flexural capacity of hybrid GFRP/steel RC beams. This model can also be used to determine the bearing capacity of GFRP RC beams.

Future research can consider the effect of concrete mixes and reinforcement arrangement on flexural behavior of the hybrid RC beams. In addition, the plastic hinge zones in concrete beams with hybrid bars could also be studied.

6. Conflicts of Interest

The authors declare no conflict of interest.

7. References

[1] Leung, H.Y., and R.V. Balendran. "Flexural Behaviour of Concrete Beams Internally Reinforced with GFRP Rods and Steel Rebars." Structural Survey 21, no. 4 (October 2003): 146–157. doi:10.1108/02630800310507159.

[2] Qu, Wenjun, Xiaoliang Zhang, and Haiqun Huang. "Flexural Behavior of Concrete Beams Reinforced with Hybrid (GFRP and Steel) Bars." Journal of Composites for Construction 13, no. 5 (October 2009): 350–359. doi:10.1061/(asce)cc.1943-5614.0000035.

[3] Lau, Denvid, and Hoat Joen Pam. "Experimental Study of Hybrid FRP Reinforced Concrete Beams." Engineering Structures 32, no. 12 (December 2010): 3857–3865. doi:10.1016/j.engstruct.2010.08.028.

[4] Mustafa, Suzan A.A., and Hilal A. Hassan. "Behavior of Concrete Beams Reinforced with Hybrid Steel and FRP Composites." HBRC Journal 14, no. 3 (December 2018): 300–308. doi:10.1016/j.hbrcj.2017.01.001.

[5] Pang, Lei, Wenjun Qu, Peng Zhu, and Jiajing Xu. "Design Propositions for Hybrid FRP-Steel Reinforced Concrete Beams." Journal of Composites for Construction 20, no. 4 (August 2016): 04015086. doi:10.1061/(asce)cc.1943-5614.0000654.

[6] Xingyu, Gu, Dai Yiqing, and Jiang Jiwang. "Flexural Behavior Investigation of Steel-GFRP Hybrid-Reinforced Concrete Beams Based on Experimental and Numerical Methods." Engineering Structures 206 (March 2020): 110117. doi:10.1016/j.engstruct.2019.110117.

[7] Bui, Linh Van Hong, Boonchai Stitmannaithum, and Tamon Ueda. "Ductility of Concrete Beams Reinforced with Both Fiber-Reinforced Polymer and Steel Tension Bars." Journal of Advanced Concrete Technology 16, no. 11 (November 14, 2018): 531–548. doi:10.3151/jact.16.531.

[8] Maranan, G.B., A.C. Manalo, B. Benmokrane, W. Karunasena, P. Mendis, and T.Q. Nguyen. "Flexural Behavior of Geopolymer-Concrete Beams Longitudinally Reinforced with GFRP and Steel Hybrid Reinforcements." Engineering Structures 182 (March 2019): 141–152. doi:10.1016/j.engstruct.2018.12.073.

[9] Kara, Ilker Fatih, Ashraf F. Ashour, and Mehmet Alpaslan Köroğlu. "Flexural Behavior of Hybrid FRP/steel Reinforced Concrete Beams." Composite Structures 129 (October 2015): 111–121. doi:10.1016/j.compstruct.2015.03.073.

[10] Kim, Seongeun, and Seunghun Kim. "Flexural Behavior of Concrete Beams with Steel Bar and FRP Reinforcement." Journal of Asian Architecture and Building Engineering 18, no. 2 (March 4, 2019): 89–97. doi:10.1080/13467581.2019.1596814.

[11] Ruan, Xiangjie, Chunhua Lu, Ke Xu, Guangyu Xuan, and Mingzhi Ni. "Flexural Behavior and Serviceability of Concrete Beams Hybrid-Reinforced with GFRP Bars and Steel Bars." Composite Structures 235 (March 2020): 111772. doi:10.1016/j.compstruct.2019.111772.

[12] Sun, Zeyang, Linchen Fu, De-Cheng Feng, Apete R. Vatuloka, Yang Wei, and Gang Wu. "Experimental Study on the Flexural Behavior of Concrete Beams Reinforced with Bundled Hybrid steel/FRP Bars." Engineering Structures 197 (October 2019): 109443. doi:10.1016/j.engstruct.2019.109443.

[13] ACI Committee. "Guide for the Design and Construction of Structural Concrete Reinforced with Fiber-Reinforced Polymer (FRP) Bars (ACI 440. 1R-15)." Farmington Hills, Michigan: American Concrete Institute (2015).

[14] Lucier, G. "Tension Tests of GFRP Bars (Prepared for: Fiber reinfor polymer Viet Nam)." North Carolina State University (2016): p. 7.

[15] Baikov, V.N. and E.E. Sigalov. "Reinforced concrete structures. General Course. Textbook for Higher Institutes of Learning, 5th Edition" (1991).

[16] Jia, B., S. Liu, X. Liu, and R. Wang. "Flexural Capacity Calculation of Hybrid Bar Reinforced Concrete Beams." Materials Research Innovations 18, no. sup2 (May 2014): S2–836–S2–840. doi:10.1179/1432891714z.000000000498.

[17] Ge, Wenjie et al. "Flexural behavior of concrete beam with hybrid reinforcement of FRP bars and steel bars." Journal of Southeast University. Natural Science Edition 42.1 (2012): 114-119.

[18] Ge, Wenjie, Jiwen Zhang, Dafu Cao, and Yongming Tu. "Flexural Behaviors of Hybrid Concrete Beams Reinforced with BFRP Bars and Steel Bars." Construction and Building Materials 87 (July 2015): 28–37. doi:10.1016/j.conbuildmat.2015.03.113.

[19] Aiello, Maria Antonietta, and Luciano Ombres. "Structural Performances of Concrete Beams with Hybrid (Fiber-Reinforced Polymer-Steel) Reinforcements." Journal of Composites for Construction 6, no. 2 (May 2002): 133–140. doi:10.1061/(asce)1090-0268(2002)6:2(133).

[20] Grace, N. F., A. K. Soliman, G. Abdel-Sayed, and K. R. Saleh. "Behavior and Ductility of Simple and Continuous FRP Reinforced Beams." Journal of Composites for Construction 2, no. 4 (November 1998): 186–194. doi:10.1061/(asce)1090-0268(1998)2:4(186).

[21] Naaman, A. and S. Jeong. “Structural ductility of concrete beams prestressed with FRP tendons.” Non-Metallic (FRP) Reinforcement for Concrete Structures: Proceedings of the Second International RILEM Symposium, Vol. 29 (23-25, August 1995).

[22] Polakowski, Natalis Horace, and Edward Joseph Ripling. "Strength and structure of engineering materials." (1966).

[23] NIIZHB named after A. A. Gvozdev. “Concrete and reinforced concrete structures. General provisions (SP 63.13330:2018).” Federal Registry of National Building Codes & Standards (2019).